NeuroImage: Clinical 25 (2020) 102110

Contents lists available at ScienceDirect

NeuroImage: Clinical

journal homepage: www.elsevier.com/locate/ynicl

Multiparametric cerebellar imaging and clinical phenotype in childhood ataxia telangiectasia

Rob A Dineen[a,b,c,*], Felix Raschke[a,d], Hannah L McGlashan[a,e], Stefan Pszczolkowski[a], Lorna Hack[a], Andrew D Cooper[b], Manish Prasad[f], Gabriel Chow[f], William P Whitehouse[f,g], Dorothee P Auer[a,b,c]

[a] Radiological Sciences, Division of Clinical Neuroscience, University of Nottingham, United Kingdom
[b] Sir Peter Mansfield Imaging Centre, University of Nottingham, United Kingdom
[c] NIHR Nottingham Biomedical Research Centre, United Kingdom
[d] Helmholtz-Zentrum Dresden - Rossendorf, Dresden, Germany
[e] School of Psychology, Faculty of Health and Behavioural Sciences, University of Queensland, Australia
[f] Nottingham Children's Hospital, Nottingham University Hospitals NHS Trust, United Kingdom
[g] Division of Child Health, University of Nottingham, United Kingdom

ARTICLE INFO

Keywords:
Ataxia telangiectasia
Magnetic resonance imaging
Magnetic resonance spectroscopy
Diffusion weighted imaging
Cerebellum

ABSTRACT

Background: Ataxia Telangiectasia (A-T) is an inherited multisystem disorder with cerebellar neurodegeneration. The relationships between imaging metrics of cerebellar health and neurological function across childhood in A-T are unknown, but may be important for determining timing and impact of therapeutic interventions.

Purpose: To test the hypothesis that abnormalities of cerebellar structure, physiology and cellular health occur in childhood A-T and correlate with neurological disability, we performed multiparametric cerebellar MRI and establish associations with disease status in childhood A-T.

Methods: Prospective cross-sectional observational study. 22 young people (9 females / 13 males, age 6.6–17.8 years) with A-T and 24 matched healthy controls underwent 3-Tesla MRI with volumetric, diffusion and proton spectroscopic acquisitions. Participants with A-T underwent structured neurological assessment, and expression / activity of ataxia-telangiectasia mutated (ATM) kinase were recorded.

Results: Ataxia-telangiectasia participants had cerebellar volume loss (fractional total cerebellar volume: 5.3% vs 8.7%, $P < 0.0005$, fractional 4th ventricular volumes: 0.19% vs 0.13%, $P < 0.0005$), that progressed with age (fractional cerebellar volumes, $r = -0.66$, $P = 0.001$), different from the control group ($t = -4.88$, $P < 0.0005$). The relationship between cerebellar volume and age was similar for A-T participants with absent ATM kinase production and those producing non-functioning ATM kinase. Markers of cerebellar white matter injury were elevated in ataxia-telangiectasia vs controls (apparent diffusion coefficient: 0.89×10^{-3} mm^2 s^{-1} vs 0.69×10^{-3} mm^2 s^{-1}, $p < 0.0005$) and correlated (age-corrected) with neurometabolite ratios indicating impaired neuronal viability (*N*-acetylaspartate:creatine $r = -0.70$, $P < 0.001$); gliosis (inositol:creatine $r = 0.50$, $P = 0.018$; combined glutamine/glutamate:creatine $r = -0.55$, $P = 0.008$) and increased myelin turnover (choline:creatine $r = 0.68$, $P < 0.001$). Fractional 4th ventricular volume was the only variable retained in the regression model predicting neurological function (adjusted $r^2 = 0.29$, $P = 0.015$).

Conclusions: Quantitative MRI demonstrates cerebellar abnormalities in children with A-T, providing non-invasive measures of progressive cerebellar injury and markers reflecting neurological status. These MRI metrics may be of value in determining timing and impact of interventions aimed at altering the natural history of A-T.

Abbreviations: ADC, Apparent Diffusion Coefficient; A-T, Ataxia Telangiectasia; ATM, Ataxia Telangiectasia mutated; A-TNEST, A-T Neurological Examination Scale Toolkit; Glx, Combined glutamine and glutamate; Ins, Inositol; MALP-EM, Multi-Atlas Label Propagation with Expectation-Maximisation based refinement; (t)Cho, (total) Choline; (t)Cr, (total) Creatine; (t)NAA, (total) N-Acetyl Aspartate

Summary Statement: Quantitative cerebellar MRI demonstrates progressive cerebellar volume loss and altered neurometabolites indicative of cerebellar injury in children and young people with ataxia telangiectasia, providing potential non-invasive markers of disease status

* Corresponding author: Room A39i, Precision Imaging Beacon, A floor, Medical School, Queen's Medical Centre, Derby Road, Nottingham, NG7 2UH, United Kingdom.

E-mail address: rob.dineen@nottingham.ac.uk (R.A. Dineen).

https://doi.org/10.1016/j.nicl.2019.102110
Received 20 August 2019; Received in revised form 7 November 2019; Accepted 25 November 2019
Available online 26 November 2019

1. Introduction

Ataxia Telangiectasia (A-T) is an autosomal recessive condition associated with cutaneous telangiectasias, cerebellar neurodegeneration, immunodeficiency, respiratory disease and increased cancer risk (Rothblum-Oviatt et al., 2016). Defects in the A-T mutated (ATM) gene lead to absent or defective production of ATM protein kinase with roles in repair of double-stranded DNA breaks and regulating cellular responses to oxidative stress (Lavin, 2008; Ditch and Paull, 2012; Chen et al., 2003). Patients with classical A-T have complete absence of ATM protein or defective ATM protein with no detectable kinase activity (Jackson et al., 2016). A-T patients who have defective ATM protein with limited kinase activity have variant A-T, and typically have milder clinical phenotype.

In classical A-T onset of clinical features occurs at median age 18 months (Devaney et al., 2017) but brain MRI scans early in the disease are often subjectively normal. In older children structural imaging studies (reviewed by Sahama et al. Sahama et al., (2014)) report cerebellar atrophy. Although studies have utilised neuroimaging techniques such as diffusion tensor imaging (Sahama et al., 2014, 2015), functional MRI (Quarantelli et al., 2013), and magnetic resonance spectroscopy (Lin et al., 2006; Wallis et al., 2007) to investigate brain structure and function in A-T, existing studies have not examined relationships between quantitative imaging findings and severity of neurological status in A-T, or between imaging metrics and age across childhood.

We aim to identify candidate imaging markers of cerebellar health and neurological disability that can be used in future treatment trials in A-T. We hypothesise that abnormalities of cerebellar structure, physiology and cellular health occur in childhood A-T and correlate with neurological disability. To test this hypothesis we use quantitative MRI measures of cerebellar volume, tissue ultrastructural integrity (apparent diffusion coefficient, ADC), and metabolic markers of neuronal viability (N-Acetyl Aspartate), cell turnover / myelin breakdown (choline), excitatory neurotransmission (combined glutamine and glutamate, Glx) and gliosis/glial activation (Inositol and Glx) from the Childhood A-T Neuroimaging Assessment Project (CATNAP). We compare metrics from children and teenagers with A-T to normally developing controls. We explore associations between cerebellar volume, water diffusion and spectroscopic measures, and perform multivariate regression analysis to identify a potential biomarker set for predicting neurological status in childhood A-T.

2. Materials and methods

2.1. Setting and participant recruitment

We conducted a single centre cross-sectional observational study set in the UK National Paediatric A-T clinic at the Nottingham Children's Hospital, a regional paediatric neurosciences centre. The study was approved by UK National Research Ethics Service (14/EM/1175). Informed consent was obtained from participants aged 16 to 18 years, and from parents/guardians of participants aged under 16 years.

Participants in the A-T group were recruited from the UK National Paediatric A-T Clinic. Inclusion criteria: Confirmed diagnosis of A-T, aged 6–18 years. Exclusion criteria: Contra-indication to MRI, concurrent or previous cancer or cancer treatment, other (non-A-T) neurological or neurosurgical condition. Healthy volunteers aged 6–18 years were recruited from local community groups, and excluded if they had contra-indication to MRI or any neurological, neurosurgical or other significant medical condition. Recruitment ran from January 2015 to September 2016. We aimed to recruit 30 participants with A-T and 20 controls. Allowing for 20% participant dropout or imaging data rejection in the A-T group this sample size permits detection of a group difference of imaging biomarkers with effect size $d = 0.52$ with 80% power and $\alpha \leq 0.05$.

2.2. Clinical assessment

A-T Neurological Examination Scale Toolkit (A-TNEST) (Jackson et al., 2016) was used to quantify neurological disability in the A-T group. A-TNEST assesses multiple neurological domains (communication, eye movements, ataxia, movement disorder, power, neuropathy), and neurology-related domains (nutrition, growth). For participants who had the A-TNEST administered in the National A-T Clinic within three months prior to the MRI scan, this score was used, otherwise the A-TNEST was performed on the day of the study visit before the scan. The A-TNEST was administered by a fully-qualified paediatric neurologist (WW, GC or MP). The total score expressed as a percentage (where 100% represents no disability) was used in the analyses. Presence of ATM kinase expression was assessed in lymphoblastoid cell lines derived from patients by western blotting. ATM kinase activity was assessed using the same patient-derived lymphoblastoid cell lines by the Taylor laboratory as described previously (Reiman et al., 2011).

2.3. MRI scanning

MRI scanning was performed on 3T Discovery MR750 (GE Healthcare, Milwaukee, WI) with 32-channel head coil, without sedation. In addition to standard paediatric MRI preparation, younger participants were shown an animation to prepare them for MRI (Szeszak et al., 2016; McGlashan et al., 2018). The multiparametric MRI scan protocol included 3D fast spoiled gradient echo T1-weighted structural MRI (1 mm isotropic resolution, TR = 8.15 ms, TE = 3.172 ms, TI = 900 ms, FOV = 256 × 256 × 156 mm); EPI-based axial diffusion-weighted imaging (participants were scanned with at least one of two sequences, a longer protocol for those tolerating the scan well: TR = 8000 ms, TE = 63 ms, $b = 1000 s/mm^2$, 32 separate non-orthogonal directions, 4 additional $b = 0$ s/mm^2 images acquired, 2 mm isotropic voxel size, whole brain coverage, number of slices = 66; or shorter protocol if not tolerating the scan well: TR = 8000 ms, TE = 83 ms, $b = 1000 s/mm^2$, 3 orthogonal directions, 0.9 mm × 0.9 mm × 4 mm voxel size, number of averages = 2, whole brain coverage, number of slices = 30); and in a subset of participants single voxel MR spectroscopy (Fig. 1) with midline cerebellar voxel location (Raschke et al., 2018) (MEGA-PRESS with GSH editing, TR = 2 s, TE = 131 ms and 128 ON and 128 OFF acquisitions; voxel dimensions $x = 50$ mm $y = 22$ mm $z = 22$ mm; spectral editing using 20 ms sinc-weighted Gaussian pulses at 7.5 ppm (OFF) and 4.54 ppm (ON)).

2.4. Image processing

T1-weighted images were segmented using Multi-Atlas Label Propagation with Expectation–Maximisation based refinement (MALP-EM) algorithm (Ledig et al., 2015; Heckemann et al., 2015), refined with an additional step to remove residual CSF from cerebellar labels by classifying all voxels in the cerebellar region with an intensity lower than a threshold (90th percentile of intensities within the 4th ventricle label) as CSF. Label volumes were recorded for cerebellar hemispheric grey matter, cerebellar hemispheric white matter, vermis lobules I–V, VI–VII and VIII–X, and 4th ventricle (Fig. 1). Cerebellar sub-regional volumes were combined to give total cerebellar volume. Volumes from all labels plus additional CSF not covered by the MALP-EM mask (obtained by means of registration and mask propagation with the Colin 27 MNI T1 template (Holmes et al., 1998)) were combined to give total intracranial volume. Cerebellar and fourth ventricular volumes were reported as fractional volumes expressed relative to total intracranial volume.

Apparent Diffusion Coefficient (ADC) maps were calculated from $b = 0$ and $b = 1000$ diffusion images using the following formula:

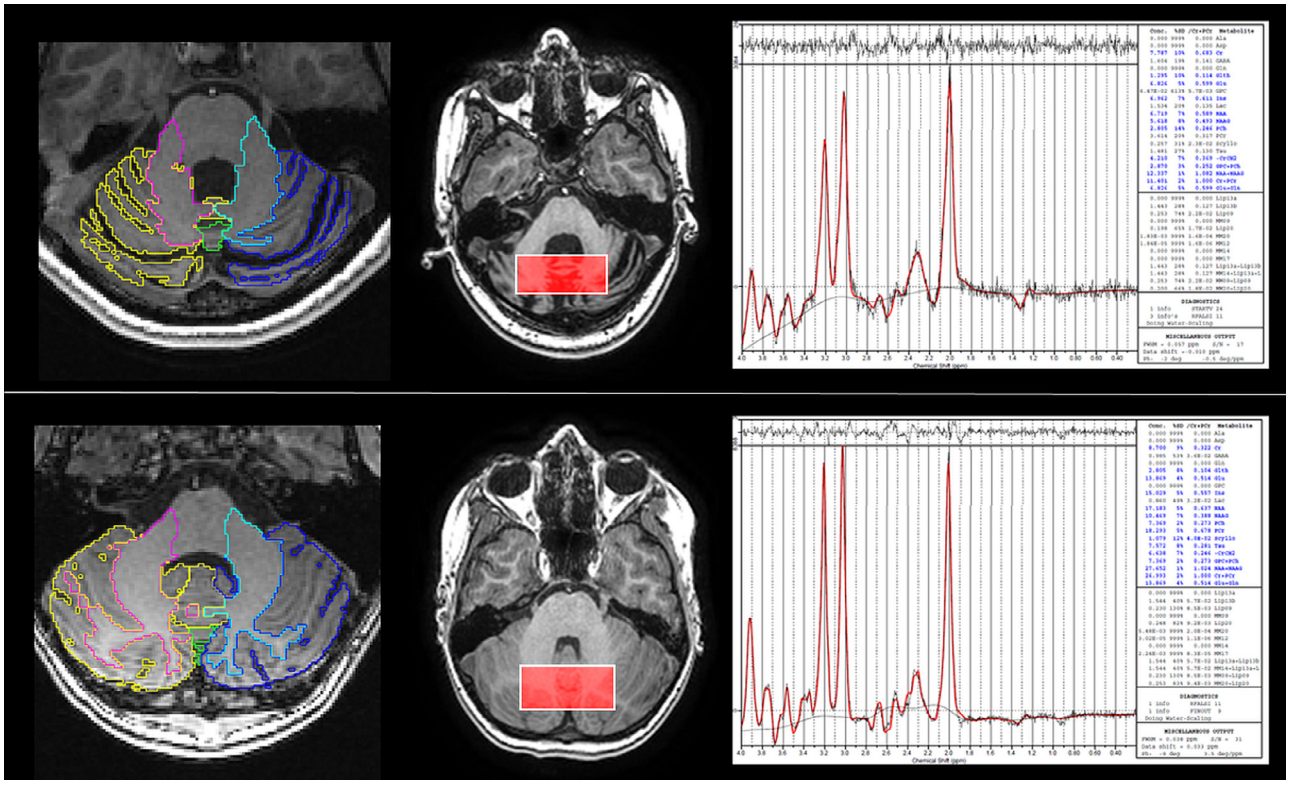

Fig. 1. Examples of magnetic resonance spectroscopy data. Examples of segmentation of structural imaging data and spectroscopy data for a participants with (top row) and without (bottom row) A-T. Left column shows the segmentation labelling for cerebellar substructures (coloured labels) overlaid on the axial T1-weighted structural image. Note the marked cerebellar atrophy in the participant with A-T. The middle column shows spectroscopy voxel position (rectangle) overlaid on axial T1-weighted structural image, with corresponding spectrum obtained shown in the right column.

$$\mathrm{ADC}(i) = \frac{\ln(b_0(i)/b_{1000}(i))}{1000} \times 10^6 = 1000 \times \ln(b_0(i)/b_{1000}(i))$$

The index i represents each voxel on the image grids and the 10^6 factor is used to transform values into units of mm^2/s. For the shorter (3-orthogonal direction) diffusion acquisitions we directly compute the ADC map using the $b = 0$ and averaged $b = 1000$ images produced automatically by the MRI scanner. In the case of longer acquisition with 32 directions, correction of eddy current distortions and subject movement was performed using the *eddy_correct* tool implemented in FSL (Jenkinson et al., 2012). We then selected the three $b = 1000$ vol corresponding to the orthogonal x, y and z directions and averaged them to subsequently compute the ADC map as above. Non-linear 10 mm spacing B-spline free-form registrations (Rueckert et al., 1999) of each ADC map to their corresponding T1-weighted image were performed using MIRTK (http://github.com/BioMedIA/MIRTK) to account for inherent spatial distortion of diffusion acquisitions. These were initialised with previously computed linear registrations. Normalised Mutual Information (Studholme et al., 1999) was utilised as similarity measure in all registrations. In the non-linear case, bending energy regularisation (Wabha, 1990) with a weight of 0.001 was applied. MALP-EM segmentation labels were used to extract mean cerebellar white matter ADC values. For participants who were able to tolerate both diffusion protocols, the absolute agreement of the cerebellar ADC values from the two acquisitions was tested using type A intraclass correlation. For these participants, the ADC calculated from the 3-direction acquisition was used in the main analysis.

Unedited MEGA-PRESS OFF spectra were analysed between 4ppm-0.2 ppm with LCModel (Version 6.3–1H) (Provencher, 2001) using a basis set simulated with TARQUIN (Wilson et al., 2011) to quantify total N-Acetyl Aspartate (tNAA), total creatine (tCr), total choline (tCho), inositol (Ins) and combined glutamine and glutamate (Glx) (Fig. 1). No relaxation correction was performed. Values for tNAA, tCho, Ins, and Glx are reported as ratios to tCr, and tNAA is additionally reported as a ratio to tCho. To allow quantification of grey matter and white matter fractions within the spectroscopy voxel, the voxel was aligned with the T1-weighted images which were subsequently segmented into grey and white matter components using SPM (http://www.fil.ion.ucl.ac.uk/spm/software/spm12). Intravoxel grey and white matter fractions were derived from aligned segmented images using in-house software.

2.5. Statistical analysis

Statistical analysis was performed using IBM SPSSv23. Normality of data distribution was assessed by Kolmorgorov-Smirnov test and inspection of histograms. Individual cases were excluded from analyses if the relevant imaging metric was not available due to incomplete acquisition or movement degradation. Group comparisons of distribution of data were by two tailed independent samples T-Test and correlation analysis by Pearson correlation unless stated otherwise. Statistical significance was defined as $\alpha < 0.05$, with Bonferroni correction applied where multiple tests were performed unless stated otherwise. Multivariate linear regression analysis was performed between MRI-derived cerebellar measures and A-TNEST. Inclusion of imaging variables as predictor variables was based on significance of $\alpha \leq 0.05$ by univariate regression with the dependent variable (A-TNEST score). Backwards removal of predictor variables was performed; the histogram of residuals and scatterplots of the standardised residual against the variable in the adjusted model were inspected to confirm assumptions of linearity and homogeneity of the data.

3. Results

The A-T group consisted of 22 children and young people (9 females

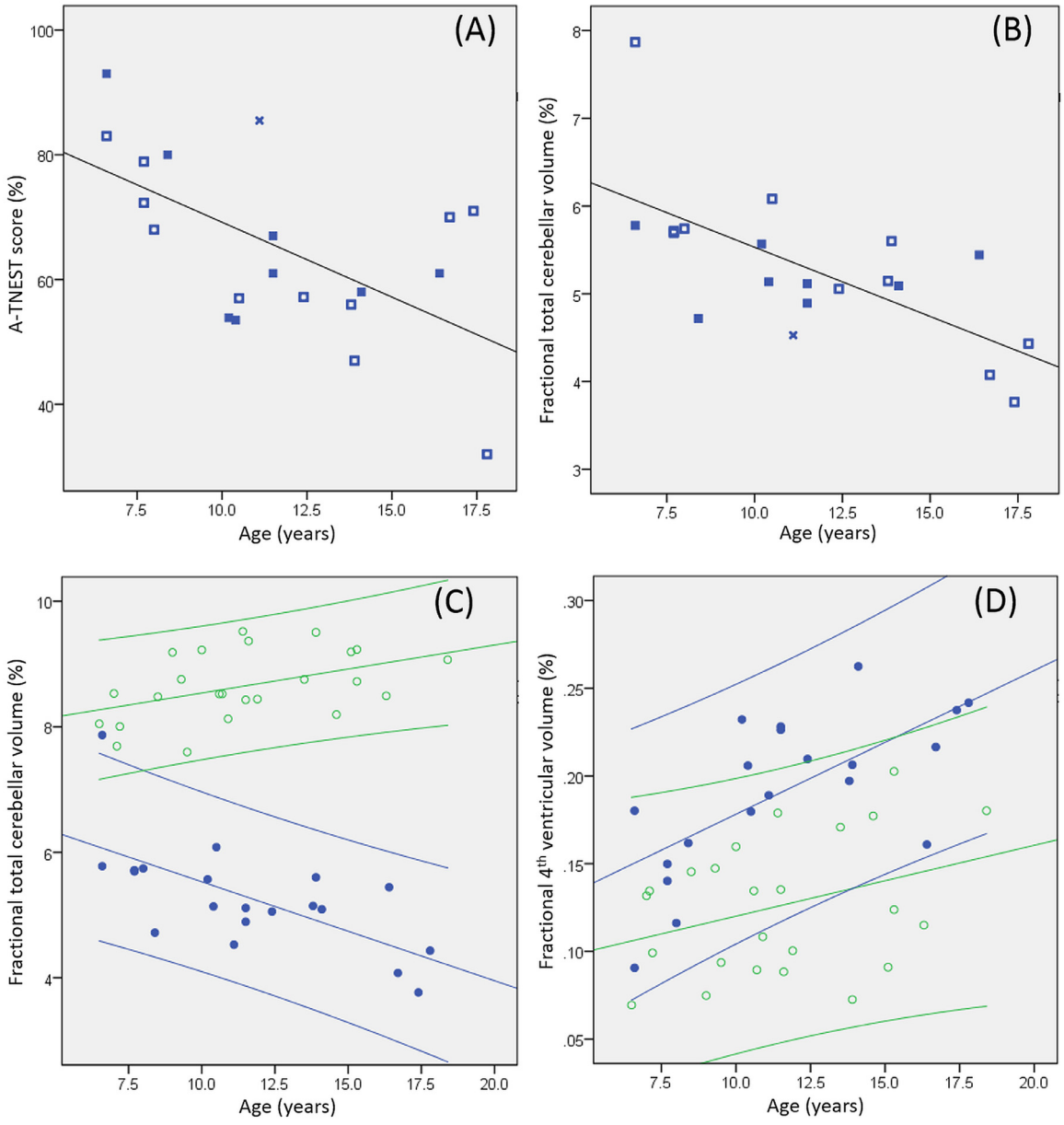

Fig. 2. Relationship of age to neurological status and cerebellar volumetry. Scatterplots of age and (A) A-TNEST score and (B) fractional total cerebellar volume for the A-T group, with line fitted for the whole group. Open squares: participants with no ATM expression; Filled squares: participants with ATM expression but no kinase activity; Star: participant with ATM expression and residual kinase activity. Scatterplot of age and (C) fractional total cerebellar volume and (D) fractional 4th ventricular volume for A-T group (filled blue circles) and control group (open green circles) with 95% confidence intervals.

/ 13 males, median age 10.8 years, range 6.6–17.8 years). Eleven had no ATM expression, 10 had ATM expression but no kinase activity, and 1 had ATM expression with some residual kinase activity. The control group comprised 24 healthy individuals (12 females/12 males, median age 11.2 years, range 6.5–18.4 years). There was no group difference in age distribution ($t = 0.006$. $P = 0.995$).

A-TNEST data were available for all participants with A-T. Median A-TNEST score was 64% (range 32%−93%) and correlated with age ($r = -0.548$, $P = 0.008$, Fig. 2A). No group difference was found in A-TNEST score for those without ATM expression and those with ATM expression but no kinase activity (mean 62.9%, s.d.14.9% vs mean 64.5%, s.d. 13.1% respectively, $P = 0.863$, Independent Samples Mann-Whitney U Test). The A-TNEST score for the participant with residual kinase activity was above scores from similarly aged children with no kinase activity (Fig. 2A).

3.1. Cerebellar volumes are smaller in childhood A-T and show negative linear correlation with age

Two structural imaging datasets were excluded from the analysis due to excessive movement. Compared to controls, participants with A-T had smaller total cerebellar volumes (mean 5.3%, s.d. 0.9% vs mean 8.7%, s.d. 0.5%, $t = -15.80$, $P < 0.005$) and larger fractional 4th ventricular volume (mean 0.19%, s.d. 0.04% vs mean 0.13%, s.d. 0.04%, $t = 5.23$, $P < 0.005$). Details of sub-regional fractional cerebellar group differences are given in Table 1.

Negative linear correlation was identified between age and fractional total cerebellar volumes for the A-T group ($r = -0.66$, $P = 0.001$, Fig. 2B), with positive correlation between these variables for the control group ($r = 0.45$, $P = 0.026$, Fig. 2C). Significant difference was found between regression coefficients for A-T and control groups ($t = -4.48$, $P < 0.0005$). Similar relationships were observed

Table 1
Group comparison of fractional total cerebellar volume, fractional sub-regional cerebellar volumes and fractional 4th ventricular volumes, showing significant differences between the A-T and healthy control groups using independent samples *T*-Test. P-values in bold significant at Bonferroni corrected $\alpha < 0.0071$.

	A-T group		Healthy controls		Independent samples *T*-Test (two tailed)	
	Mean	S.D.	Mean	S.D.	*t*	*P*
Fractional total cerebellar volume	5.3%	0.9%	8.7%	0.5%	−15.80	$\mathbf{2.8 \times 10^{-19}}$
Fractional cerebellar hemisphere grey matter volume	3.5%	0.6%	6.0%	0.4%	−15.71	$\mathbf{3.4 \times 10^{-19}}$
Fractional cerebellar hemisphere white matter volume	1.5%	0.3%	2.1%	0.3%	−7.07	$\mathbf{1.2 \times 10^{-8}}$
Fractional vermis lobule I-V volume	0.15%	0.03%	0.28%	0.03%	−13.73	$\mathbf{4.0 \times 10^{-17}}$
Fractional vermis lobule VI-VII volume	0.06%	0.01%	0.11%	0.02%	−9.06	$\mathbf{2.0 \times 10^{-11}}$
Fractional vermis lobule VIII-X volume	0.10%	0.03%	0.18%	0.02%	−11.43	$\mathbf{1.8 \times 10^{-14}}$
Fractional 4th ventricular volume	0.19%	0.04%	0.13%	0.04%	5.23	$\mathbf{5 \times 10^{-6}}$

S.D. = Standard Deviation.

for fractional cerebellar sub-regional volumes (Supplementary fig. 1A-E). The relationship between cerebellar volume and age was similar for A-T participants with absent ATM kinase and those producing non-functioning ATM kinase (Fig. 2B). Positive correlation was found between age and fractional 4th ventricular volume for the A-T group ($r = 0.66$, $P = 0.001$) but not the control group ($r = 0.34$, $P = 0.10$) (Fig. 2D), but no group difference was found between regression coefficients.

3.2. Cerebellar diffusion is abnormal in childhood A-T independent of cerebellar volume and age

Diffusion data were available for 19 participants in the A-T group and all control participants. Cerebellar white matter ADC values were elevated in the A-T group compared to controls (adjusted means $0.89 \times 10^{-3}\,mm^2\,s^{-1}$ vs $0.69 \times 10^{-3}\,mm^2\,s^{-1}$ respectively, ANCOVA treating diffusion-weighted imaging acquisition method as a covariate of no interest, $F = 39.6$, $P < 0.0005$). Cerebellar white matter ADC did not correlate with age or fractional cerebellar volume for either group. For the 24 participants who underwent both diffusion protocols, the type A intraclass correlation using an absolute agreement definition for cerebellar white matter ADC values was $r = 0.75$, $P = 0.001$.

3.3. Cerebellar metabolites are altered in childhood A-T independent of cerebellar volume and age

Twenty-three participants had good quality cerebellar spectroscopy data (12 with A-T, mean age 11.5 years, s.d. 4.1 years; 11 without A-T, mean age 12.5 years, s.d. 2.8 years; no group difference in age distribution: $t = -0.681$. $P = 0.50$). No difference was found between A-T and control groups for the ratio of grey matter to white matter within the spectroscopy voxel (mean 2.37, s.d. 0.81 vs mean 2.63, s.d. 0.55 respectively, $P = 0.091$, Independent Samples Mann–Whitney U Test). Comparison of metabolite ratios using independent samples Mann-Whitney U test due to non-normal distributions showed significant group differences (following Bonferroni correction) for tNAA/tCr, tCho/tCr and tNAA/tCr (Table 2). No significant correlations were identified between metabolite ratios and age or fractional cerebellar volume for either the A-T or control groups using Spearman's Rho.

3.4. Cerebellar metabolite ratios correlate with ultrastructural white matter integrity in childhood A-T and healthy controls

Partial correlation (controlling for age) showed positive correlation between mean cerebellar white matter ADC and tCho/tCr ($r_{partial} = 0.68$, $P < 0.001$) and negative correlations with tNAA/tCr ($r_{partial} = -0.70$, $P < 0.001$), Glx/tCr ($r_{partial} = -0.55$, $P = 0.008$) and tNAA/tCho ($r_{partial} = -0.66$, $P = 0.001$) (Fig. 3). Positive correlation between mean cerebellar white matter ADC and Ins/tCr ($r_{partial} = 0.50$, $P = 0.018$) was not significant at the Bonferroni corrected $\alpha < 0.0083$.

Table 2
Cerebellar metabolite changes in A-T. Metabolite ratios and statistical testing of group differences using Mann–Whitney *U* test are shown. P–values in bold significant at Bonferroni corrected α-value < 0.0083.

	A-T group		Healthy controls		Mann–Whitney *U*
	Median	Range	Median	Range	*P*
tNAA/tCr	0.99	0.91–1.39	1.11	1.02–1.17	**0.002**
tCho/tCr	0.30	0.19–0.34	0.27	0.24–0.29	**0.007**
Ins/tCr	0.65	0.55–0.83	0.62	0.56–0.68	0.118
Glx/tCr	0.48	0.43–0.66	0.54	0.49–0.65	0.037
GSH/tCr	0.11	0.07–0.17	0.12	0.11–0.13	0.118
tNAA/tCho	3.22	2.83–7.35	4.23	3.71–4.58	**0.002**

tNAA = total N-Acetyl Aspartate, tCr = total creatine, tCho = total choline, Ins = inositol, Glx = combined glutamine and glutamate, GSH = glutathione.

3.5. Fourth ventricular volume correlates with neurological status in childhood A-T

Results of univariate analysis between cerebellar MRI metrics and neurological status are shown in Table 3. Three MRI-derived measures met criterion for inclusion in the regression analysis by univariate analysis: Fractional 4th ventricular volume ($r = -0.53$, $P = 0.015$), fractional vermis lobules I-V volume ($r = 0.46$, $P = 0.041$) and Glx/tCr ($r = 0.59$, $P = 0.045$) (Fig. 4). However, inclusion of Glx/tCr would have limited the analysis to 12 instead of 20 participants, hence this variable was excluded. The final adjusted model consisted only of fractional 4th ventricular volume achieving $r^2_{adjusted} = 0.29$, $P = 0.015$ (unstandardized coefficient $B = -17{,}456$, standard error of $B = 6523$, 95% confidence intervals of B: −31,160 to −3751).

4. Discussion

We identified age-related profoundly progressive cerebellar volume loss in children and young people with A-T compared to a small linear volume increase in healthy individuals. The divergence is most marked for total cerebellar volume, cerebellar grey matter volumes and superior vermian lobule volumes, but divergence was identified for all cerebellar sub-regions. Our observation that 95% confidence intervals separate towards the end of the first decade (Fig. 2C) is consistent with clinical experience that cerebellar atrophy can be difficult to detect by visual inspection of diagnostic MRI scans in the first few years of life for children subsequently confirmed to have A-T, and this may contribute to reported delays in diagnosis of A-T (Devaney et al., 2017). The relationship between cerebellar volume and age was similar for A-T participants with absent ATM kinase production and those producing non-functioning ATM kinase.

Despite the linear relationship between age and fractional cerebellar volume in the A-T group, we did not find correlation between fractional total cerebellar volume and neurological status. We did identify linear relationships between neurological status and both fractional superior vermian lobule volumes and fractional fourth ventricular volume in

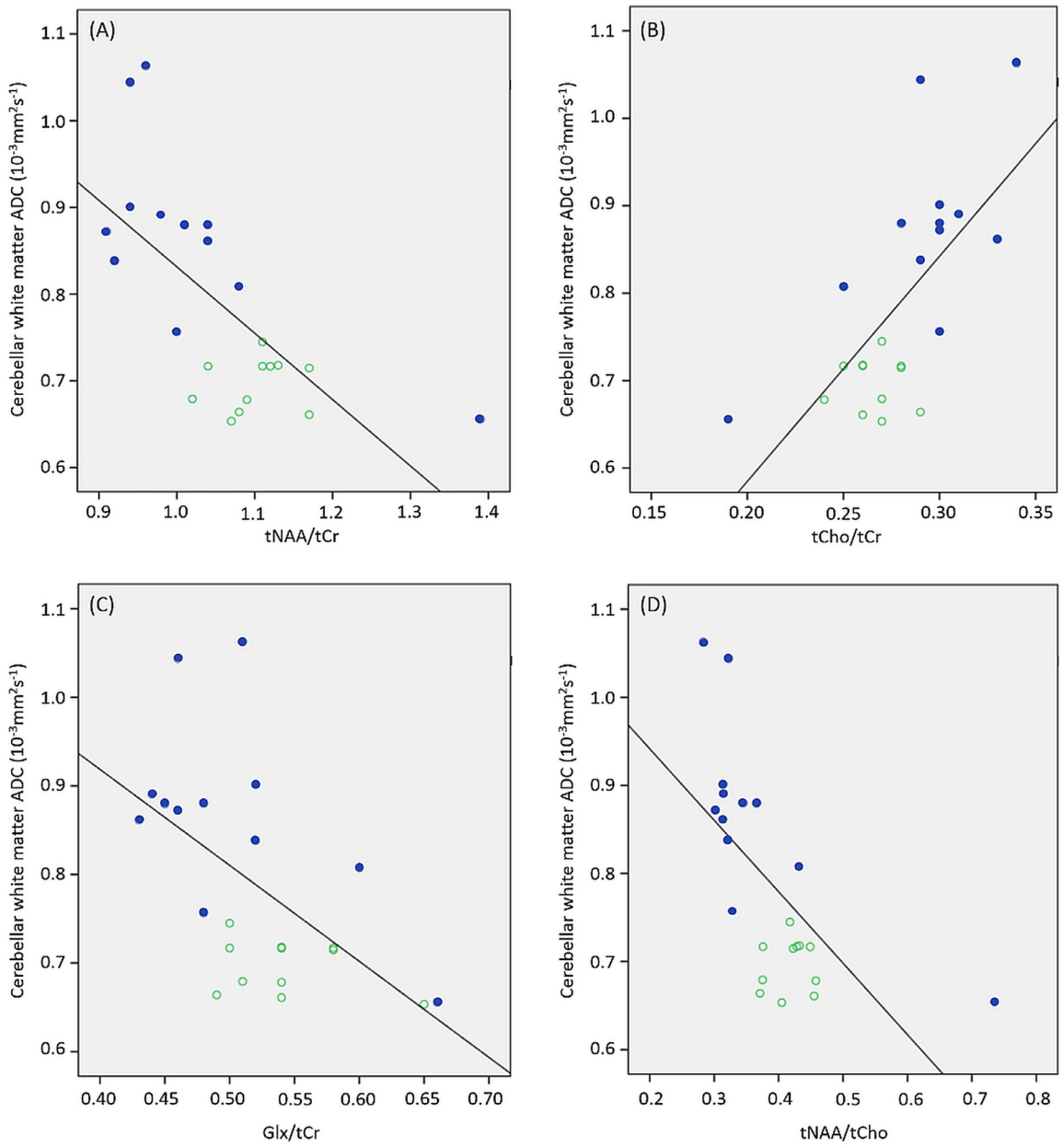

Fig. 3. Correlations between cerebellar neurometabolites and white matter apparent diffusion coefficient. Scatterplots showing correlations between cerebellar white matter ADC and (A) tNAA/tCr, (B) tCho/tCr, (C) Glx/tCr and (D) tNAA/tCho. A-T group: filled blue circles; Control group: open green circles.

univariate analysis of 20 participants, with fractional fourth ventricular volume surviving as sole predictor variable for neurological status in multivariate regression analysis. Although it is surprising that cerebellar atrophy is not the strongest correlate of neurological dysfunction, there are potential explanations. The A-TNEST score captures a number of aspects of neurological function, including domains that are not specifically cerebellar, such as extra-pyramidal movement abnormalities. We observed that fractional 4th ventricular volume increased significantly with age in the A-T but not control group, which is likely to be dominated by atrophy of surrounding cerebellar structures including the vermis, cerebellar peduncles, but could also capture subtle atrophy of the dorsal pons, medulla and midbrain. The combination of atrophy of these structures may drive neurological symptoms in A-T explaining the observed correlation with A-TNEST that was not identified for fractional total cerebellar volume alone.

We demonstrate significant elevation of cerebellar white matter ADC in childhood A-T and significant alterations in cerebellar metabolite levels, independent of age and cerebellar volume. ADC provides an index of water mobility, and elevation implies pathological alterations in tissue ultrastructure or increase tissue water content. Sahama and colleagues identified elevated mean diffusivity, a diffusion tensor imaging derived metric related to ADC, in the left cerebellar hemispheric white matter and right superior cerebellar lobule of 11 people with A-T, consistent with our findings (Sahama et al., 2014b). This group elegantly demonstrate that loss of white matter integrity extends beyond the cerebellum, with diffusion metrics indicating degeneration along corticomotor, corticospinal and somatosensory pathways (Sahama et al., 2015).

Reduction of cerebellar tNAA ratios was found in the A-T group, using a voxel including cerebellar grey and white matter. tNAA depletion indexes neuronal dysfunction and death (Geiszler et al., 2018), and our findings are consistent with classical descriptions of cerebellar grey matter pathology in A-T including loss of Purkinje and granular cells (Clark et al., 2015). We found tNAA ratios correlated inversely

Table 3
Univariate analysis between cerebellar MRI metrics and neurological status in the A-T group. P-values in bold significant at uncorrected $\alpha < 0.05$.

	n	*r*	*P*
Fractional total cerebellar volume	20	0.22	0.362
Fractional cerebellar hemisphere grey matter volume	20	0.1	0.572
Fractional cerebellar hemisphere white matter volume	20	0.28	0.233
Fractional vermis lobules I-V volume	20	0.46	**0.041**
Fractional vermis lobules VI-VII volume	20	0.06	0.802
Fractional vermis lobules VIII-X volume	20	0.38	0.096
Fractional 4th ventricular volume	20	−0.53	**0.015**
Cerebellar white matter ADC	19	−0.27	0.266
tNAA/tCr	12	0.41*	0.185
tCho/tCr	12	−0.20*	0.526
Ins/tCr	12	0.17*	0.595
Glx/tCr	12	0.59*	**0.045**
GSH/tCr	12	0.11*	0.742
tNAA/tCho	12	0.36*	0.255

* Spearmann rank correlation used in view of small sample size; elsewhere Pearson correlation used. ADC = apparent diffusion coefficient, tNAA = total N-Acetyl Aspartate, tCr = total creatine, tCho = total choline, Ins = inositol, Glx = combined glutamine and glutamate, GSH = glutathione.

with cerebellar white matter ADC indicating that loss of integrity of cerebellar white matter ultrastructure mirrors neuronal failure, although the causal nature of this association is not clear. The fact that neither of these measures correlates with cerebellar volume suggests ultrastructural disruption and neuronal dysfunction are not directly reflected by cerebellar volume changes. Our finding of cerebellar tNAA depletion replicates previous findings in A-T (Lin et al., 2006; Wallis et al., 2007), and in particular that reduction in cerebellar tNAA relative to choline distinguishes people with A-T from healthy controls. (Wallis et al., 2007)

We demonstrate elevated choline ratios childhood A-T (confirming previous findings in adult A-T (Wallis et al., 2007)), and show positive correlation of tCho/tCr with cerebellar white matter ADC. Choline elevation is a marker of myelin turnover observed in conditions associated with demyelination (Bitsch et al., 1999), and our findings are consistent with reports of demyelination in A-T (Terplan and Krauss, 1969). ADC is non-specific and indexes alterations in multiple ultrastructural tissue components, but elevated water diffusion is recognised in diseases associated with demyelination (Bammer et al., 2000) which may explain the observed correlation with choline ratios.

Rodent models of A-T demonstrate primary abnormalities of astrocytic cells including slow growth, premature senescence and evidence of oxidative stress (Meshulam et al., 2012; Gosink et al., 1999; Liu et al., 2005). Our results support astroglial abnormalities in A-T; we found positive correlation (uncorrected $P < 0.05$) between inositol and cerebellar white matter ADC, and mean inositol ratios were higher in the A-T group although the distribution was not significantly different between groups. Inositol is elevated in diseases associated with astrogliosis with recent evidence suggesting inositol elevation may be a relatively late occurrence in the neurodegeneration-related inflammatory cascade (Geiszler et al., 2018). We identified lower cerebellar combined glutamine and glutamate (Glx) ratios in the A-T group than controls (uncorrected $P < 0.05$) and correlation between cerebellar Glx ratios and cerebellar white matter ADC, linking glutamine/glutamate metabolism to underlying tissue integrity in A-T. Although Glx concentrations may relate to proportions of grey and white matter in the sampled volume (Bustillo et al., 2017) this is unlikely to be driving our results as we found no group difference in grey:white matter ratio in the spectroscopy voxel. Altered glutamate homeostasis co-occurs with glial activation in the context of neurodegeneration, with reduced glutamine and elevated glutamate associated with increased levels of glutamate dehydrogenase in animal models of progressive neurodegeneration (Geiszler et al., 2018). Recent work has shown low serum levels of the glutamate precursor glutamine in ATM-deficient mice, and altered expression of genes related to glutamine metabolism in ATM-deficient mice and humans with A-T (Chen et al., 2016). Our findings support a role for altered glutamine/glutamate metabolism in A-T but our spectroscopy protocol was not designed to resolve glutamine and glutamate separately limiting our ability to explore pathological mechanisms.

Despite being one of the largest studies using advanced MRI techniques to study childhood A-T, the analysis is limited by small numbers. The rarity of A-T makes it difficult to assemble large cohorts; Multicentre and international collaborations are required to allow sufficient numbers for comprehensive statistical analysis, but this will introduce challenges relating to standardisation of multiparametric MRI protocols (Ashton and Riek, 2013). Our study focusses on cerebellar imaging metrics, but we acknowledge that pathological changes in the cerebrum and spinal cord (Clark et al., 2015) could contribute to neurological disability. Another potential limitation is the use of two diffusion protocols, a pragmatic decision made because some participants could not tolerate the longer 32-direction protocol and were scanned with a shorter 3-direction protocol. Previous work shows good reproducibility of ADC values between different scanners and protocols, (Grech-Sollars et al., 2015) and from the 24 participants who underwent both diffusion protocols in our study, we find a high intraclass correlation using an absolute agreement definition for the cerebellar white matter ADC values. In addition, we controlled for choice of diffusion protocol in group comparison of ADC values.

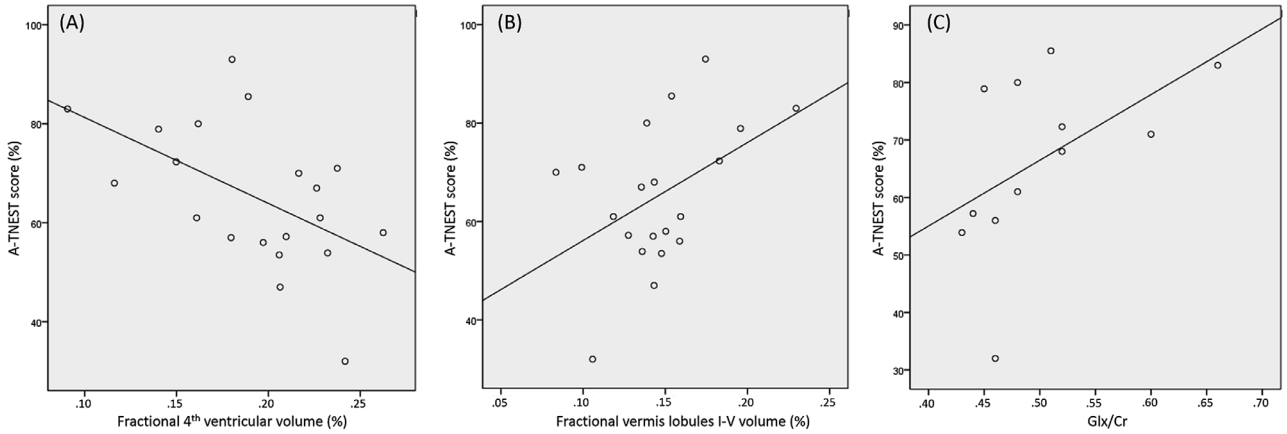

Fig. 4. Relationship of neurological status to imaging variables. Scatterplots for the three imaging variable showing correlation with A-TNEST score on univariate analysis for the A-T group; (A) fractional 4th ventricular volume, (B) fractional vermis lobules I-V volumes and (C) Glx/tCr.

5. Conclusion

Quantitative cerebellar MRI demonstrates differences between children with A-T and controls, provide measures of progressive cerebellar neurodegeneration, and can provide imaging markers of neurological status in childhood A-T. Alterations in metabolites known to be related to neuronal viability, glial activation and myelin turnover relate to loss of cerebellar white matter ultrastructural integrity in childhood A-T. As novel treatment strategies are developed and tested (Chessa et al., 2014), these MRI metrics may be of value in determining timing and impact of interventions aimed at altering the natural history of A-T.

Funding

The funding for the research was from a research grant awarded jointly by A-T Children's Project and Action for A-T [grant ref: The CATNAP Study]. The funder had no role in the study design; the collection, analysis and interpretation of data; the writing of the report; and the decision to submit the article for publication.

Acknowledgements

The authors would like to thank the children, young people and families who participated in the CATNAP study. We also gratefully acknowledge the support William Davis and Kay Atkins at the AT Society for support with publicising the study and arranging schedules and transport for participant visits; Dr Min Ong for additional support with neurological assessments.

Supplementary materials

Supplementary material associated with this article can be found, in the online version, at doi:10.1016/j.nicl.2019.102110.

References

Ashton, E., Riek, J, 2013. Advanced MR techniques in multicenter clinical trials. J. Magn. Reson. Imaging 37 (4), 761–769. https://doi.org/10.1002/jmri.23799.

Bammer, R., Augustin, M., Strasser-Fuchs, S., et al., 2000. Magnetic resonance diffusion tensor imaging for characterizing diffuse and focal white matter abnormalities in multiple sclerosis. Magn. Reson. Med. 44 (4), 583–591.

Bitsch, A., Bruhn, H., Vougioukas, V., et al., 1999. Inflammatory CNS demyelination: histopathologic correlation with in vivo quantitative proton MR spectroscopy. AJNR Am. J. Neuroradiol. 20 (9), 1619–1627.

Bustillo, J.R., Jones, T., Chen, H., et al., 2017. Glutamatergic and neuronal dysfunction in gray and white matter: a spectroscopic imaging study in a large schizophrenia sample. Schizophr. Bull. 43 (3), 611–619. https://doi.org/10.1093/schbul/sbw122.

Chen, J., Chen, Y., Vail, G., et al., 2016. The impact of glutamine supplementation on the symptoms of ataxia-telangiectasia: a preclinical assessment. Mol. Neurodegener. 11 (1), 60. https://doi.org/10.1186/s13024-016-0127-y. [published Online First: 2016/08/18].

Chen, K., Albano, A., Ho, A., et al., 2003. Activation of p53 by oxidative stress involves platelet-derived growth factor-beta receptor-mediated ataxia telangiectasia mutated (ATM) kinase activation. J. Biol. Chem. 278 (41), 39527–39533. https://doi.org/10.1074/jbc.M304423200. [published Online First: 2003/07/30].

Chessa, L., Leuzzi, V., Plebani, A., et al., 2014. Intra-erythrocyte infusion of dexamethasone reduces neurological symptoms in ataxia teleangiectasia patients: results of a phase 2 trial. Orphanet. J. Rare. Dis. 9, 5. https://doi.org/10.1186/1750-1172-9-5. [published Online First: 2014/01/09].

Clark, H.B, et al., 2015. Degenerative ataxic disorders. In: Love, S, Budka, H, Ironside, JW (Eds.), Greenfield's Neuropathology, 9th Edition ed: CRC Press, pp. 799–816.

Devaney, R., Pasalodos, S., Suri, M., et al., 2017. Ataxia telangiectasia: presentation and diagnostic delay. Arch. Dis. Child. 102 (4), 328–330. https://doi.org/10.1136/archdischild-2016-310477.

Ditch, S., Paull, T.T, 2012. The ATM protein kinase and cellular redox signaling: beyond the DNA damage response. Trends Biochem. Sci. 37 (1), 15–22. https://doi.org/10.1016/j.tibs.2011.10.002. [published Online First: 2011/11/11].

Geiszler, P.C., Ugun-Klusek, A., Lawler, K., et al., 2018. Dynamic metabolic patterns tracking neurodegeneration and gliosis following 26S proteasome dysfunction in mouse forebrain neurons. Sci. Rep. 8 (1), 4833. https://doi.org/10.1038/s41598-018-23155-2. [published Online First: 2018/03/19].

Gosink, E.C., Chong, M.J., McKinnon, P.J, 1999. Ataxia telangiectasia mutated deficiency affects astrocyte growth but not radiosensitivity. Cancer Res. 59 (20), 5294–5298.

Grech-Sollars, M., Hales, P.W., Miyazaki, K., et al., 2015. Multi-centre reproducibility of diffusion MRI parameters for clinical sequences in the brain. NMR Biomed. 28 (4), 468–485. https://doi.org/10.1002/nbm.3269.

Heckemann, R.A., Ledig, C., Gray, K.R., et al., 2015. Brain extraction using label propagation and group agreement: pincram. PLoS ONE 10 (7), e0129211. https://doi.org/10.1371/journal.pone.0129211.

Holmes, C.J., Hoge, R., Collins, L., et al., 1998. Enhancement of MR images using registration for signal averaging. J. Comput. Assist. Tomogr. 22 (2), 324–333.

Jackson, T.J., Chow, G., Suri, M., et al., 2016. Longitudinal analysis of the neurological features of ataxia-telangiectasia. Dev. Med. Child Neurol. 58 (7), 690–697. https://doi.org/10.1111/dmcn.13052.

Jenkinson, M., Beckmann, C.F., Behrens, T.E., et al., 2012. FSL. Neuroimage 62 (2), 782–790. https://doi.org/10.1016/j.neuroimage.2011.09.015. [published Online First: 2011/09/16].

Lavin, M.F, 2008. Ataxia-telangiectasia: from a rare disorder to a paradigm for cell signalling and cancer. Nat. Rev. Mol. Cell Biol. 9 (10), 759–769. https://doi.org/10.1038/nrm2514.

Ledig, C., Heckemann, R.A., Hammers, A., et al., 2015. Robust whole-brain segmentation: application to traumatic brain injury. Med. Image Anal. 21 (1), 40–58. http://dx.doi.org/10.1016/j.media.2014.12.003.

Lin, D.D., Crawford, T.O., Lederman, H.M., et al., 2006. Proton MR spectroscopic imaging in ataxia-telangiectasia. Neuropediatrics 37 (4), 241–246. https://doi.org/10.1055/s-2006-924722.

Liu, N., Stoica, G., Yan, M., et al., 2005. ATM deficiency induces oxidative stress and endoplasmic reticulum stress in astrocytes. Lab. Invest. 85 (12), 1471–1480. https://doi.org/10.1038/labinvest.3700354.

McGlashan, H.L., Dineen, R.A., Szeszak, S., et al., 2018. Evaluation of an internet-based animated preparatory video for children undergoing non-sedated MRI. Br. J. Radiol. https://doi.org/10.1259/bjr.20170719. 20170719[published Online First: 2018/05/10].

Meshulam, L., Galron, R., Kanner, S., et al., 2012. The role of the neuro-astro-vascular unit in the etiology of ataxia telangiectasia. Front Pharmacol. 3, 157. https://doi.org/10.3389/fphar.2012.00157. [published Online First: 2012/09/17].

Provencher, S.W., 2001. Automatic quantitation of localized in vivo ^{1}H spectra with LCModel. NMR Biomed. 14 (4), 260–264.

Quarantelli, M., Giardino, G., Prinster, A., et al., 2013. Steroid treatment in Ataxia-Telangiectasia induces alterations of functional magnetic resonance imaging during prono-supination task. Eur. J. Paediatr. Neurol. 17 (2), 135–140. https://doi.org/10.1016/j.ejpn.2012.06.002. [published Online First: 2012/07/02].

Raschke, F., Noeske, R., Dineen, R.A., et al., 2018. Measuring cerebral and cerebellar glutathione in children using. AJNR Am. J. Neuroradiol. 39 (2), 375–379. https://doi.org/10.3174/ajnr.A5457. [published Online First: 2017/12/14].

Reiman, A., Srinivasan, V., Barone, G., et al., 2011. Lymphoid tumours and breast cancer in ataxia telangiectasia; substantial protective effect of residual ATM kinase activity against childhood tumours. Br. J. Cancer 105 (4), 586–591. https://doi.org/10.1038/bjc.2011.266. [published Online First: 2011/07/26].

Rothblum-Oviatt, C., Wright, J., Lefton-Greif, M.A., et al., 2016. Ataxia telangiectasia: a review. Orphanet. J. Rare. Dis. 11 (1), 159. https://doi.org/10.1186/s13023-016-0543-7. [published Online First: 2016/11/25].

Rueckert, D., Sonoda, L.I., Hayes, C., et al., 1999. Nonrigid registration using free-form deformations: application to breast MR images. IEEE Trans. Med. Imaging 18 (8), 712–721. https://doi.org/10.1109/42.796284.

Sahama, I., Sinclair, K., Fiori, S., et al., 2014b. Altered corticomotor-cerebellar integrity in young ataxia telangiectasia patients. Mov. Disord. 29 (10), 1289–1298. https://doi.org/10.1002/mds.25970. [published Online First: 2014/07/17].

Sahama, I., Sinclair, K., Fiori, S., et al., 2015. Motor pathway degeneration in young ataxia telangiectasia patients: a diffusion tractography study. Neuroimage. Clin. 9, 206–215. https://doi.org/10.1016/j.nicl.2015.08.007. [published Online First: 2015/08/20].

Sahama, I., Sinclair, K., Pannek, K., et al., 2014a. Radiological imaging in ataxia telangiectasia: a review. Cerebellum 13 (4), 521–530. https://doi.org/10.1007/s12311-014-0557-4.

Studholme, C., Hill, D., Hawkes, D., 1999. An overlap invariant entropy measure of 3D medical image alignment. Pattern Recognit. 32 (1), 71–86.

Szeszak, S., Man, R., Love, A., et al., 2016. Animated educational video to prepare children for MRI without sedation: evaluation of the appeal and value. Pediatr. Radiol. 46 (12), 1744–1750. https://doi.org/10.1007/s00247-016-3661-4. [published Online First: 2016/08/27].

Terplan, K.L., Krauss, R.F, 1969. Histopathologic brain changes in association with ataxia-telangiectasia. Neurology 19 (5), 446–454.

Wabha, G, 1990. Spline Models For Observational Data. CBMS-NSF Regional Conference Series in Applied Mathematics, Philadelphia.

Wallis, L.I., Griffiths, P.D., Ritchie, S.J., et al., 2007. Proton spectroscopy and imaging at 3T in ataxia-telangiectasia. AJNR Am. J. Neuroradiol. 28 (1), 79–83.

Wilson, M., Reynolds, G., Kauppinen, R.A., et al., 2011. A constrained least-squares approach to the automated quantitation of in vivo 1H magnetic resonance spectroscopy data. Magn. Reson. Med. 65 (1), 1–12. https://doi.org/10.1002/mrm.22579.